ACS OMEGA

Open Access

http://pubs.acs.org/journal/acsodf

Article

Miscibility Characteristics of CO_2−Oil in Tight Sandstone Reservoirs: Insights from Molecular Dynamics Simulations

Fangna Liu,* Xiangzeng Wang,* Hong Yang, Quansheng Liang, Ying Liu, and Zhenjie Yao

Cite This: *ACS Omega* 2024, 9, 15663−15676

Read Online

ACCESS | Metrics & More | Article Recommendations

ABSTRACT: Identifying the microscopic mechanism of CO_2−oil miscibility is significant for the CO_2 enhanced oil recovery (CO_2−EOR) in tight sandstone reservoirs. In this work, the effects of oil composition, formation pressure, temperature, and methane content on the characteristics of the CO_2−oil miscibility were systematically studied by molecular simulation methods. According to the change of oil−gas centroid displacement, the CO_2−oil miscibility behavior was divided into four stages: rapid diffusion, CO_2 dissolution and oil swelling, competitive adsorption and oil film detachment, and complete miscibility or dynamic equilibrium stability. The results showed that light or medium component oil is more easily miscible with CO_2 under reservoir conditions. The changes in temperature and pressure will greatly influence the oil−gas miscibility. Increasing the temperature is conducive to reducing the adsorption energy between oil and quartz, thus improving the miscibility of CO_2 and heavy component oil. However, the static swelling effects of CO_2 alone cannot effectively displace the heavy component oil on quartz. The CO_2 diffusion coefficient perpendicular to the quartz surface does not increase continuously with the temperature increase due to the adsorption of oil and quartz. There is a critical temperature range of 320−340 K, which makes the miscibility effects the best. A small amount of CH_4 can enhance the interaction energy between the two phases of oil and gas, thus promoting the miscibility of CO_2 and oil at the interface. However, it is not conducive to oil film detachment, with the CH_4 content increasing.

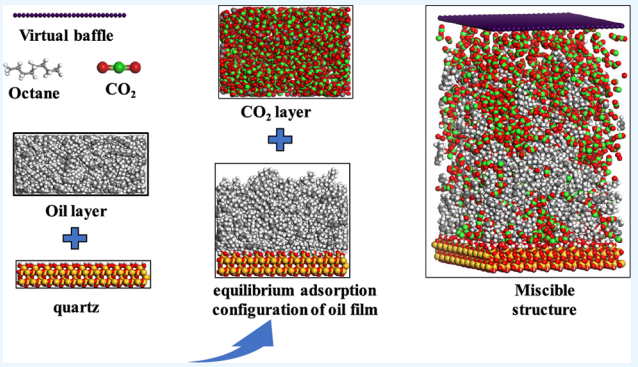

1. INTRODUCTION

With the continuous growth of the world's demand for oil and gas resources and the continuous decline of conventional oil and gas production, unconventional oil and gas have become the focus of global oil and gas exploration and development.[1−3] The Ordos Basin is rich in tight oil and gas resources and has great development prospects. However, due to the characteristics of the poor physical properties, small pore throat, and serious heterogeneity of tight reservoirs, problems such as high water injection pressure and poor oil recovery can easily be caused in the development process.[4] As the main technology of tertiary oil recovery, CO_2 flooding has significant advantages in tight oil reservoir development due to its better injection capacity and dissolution characteristics[5−11] and has been widely used in oil field practice.[12−18] At the same time, as one of the main ways to achieve carbon neutrality, CO_2 flooding is also conducive to achieving the double benefits of enhanced oil recovery and carbon emission reduction.[19−22] Therefore, it is necessary to further clarify the miscibility mechanism of CO_2 and oil in tight sandstone reservoirs.

Micronanopore throat structures are widely developed in tight sandstone reservoirs.[23,24] The high specific-surface area of micronano scale channels makes the interaction between fluid molecules and solid walls more significant.[25,26] The mechanism of CO_2−EOR includes not only dissolution and swelling, reduction of oil viscosity, reduction of interfacial tension, extraction of light components, and change of reservoir physical properties and wettability alteration but also competitive adsorption and oil film detachment. Currently, the interaction mechanism between CO_2 and oil has been studied through many physical experiments and numerical simulations. Seyyedi et al.[27] used the flow visualization experiments to explore the microscopic process of CO_2 flooding. They revealed that during the interaction between CO_2 and oil, the formation and growth of the new gaseous phase of multicomponent mixture was the main reason for the additional oil recovery. The new gaseous phase led to a much larger oil swelling and thereby the isolated oil could be reconnected and redistributed, so as to promote the further increase of the miscible region. This study explained the

Received: January 18, 2024
Revised: February 21, 2024
Accepted: March 1, 2024
Published: March 18, 2024

transition law of the mobile phase and residual phase oil in detail and clarified the displacement law of oil in the confined space. Li et al.[28] explored the interaction mechanism, seepage characteristics, and residual oil distribution between CO_2 and oil under an in situ formation environment through the microfluidic experimental platform. The microscopic interaction mechanism of dissolution, swelling, extraction, and mixing between CO_2 and oil was revealed. Samara et al.[29] confirmed that the solubility of CO_2 in the aqueous phase impacts both IFT and volumetric expansion though experiments, and they presented a new method to infer CO_2 solubility in the oleic phase, based on volumetric expansion and density data. To reveal the differences in oil and gas migration rules under different injection modes, Zhang et al.[30] used optical microscopy and high-speed photography techniques to observe the changes in the oil−gas−water three-phase interface in the process of CO_2 injection in real-time. With the increase of gas production, the associated gas reinjection technology has attracted wide attention. Previous studies had examined the impacts of CH_4 in the CO_2 stream upon the minimum miscibility pressure (MMP). They found that the presence of CH_4 would increase the MMP compared to that of CO_2, thus negatively impacting the miscibility and EOR performance.[31−34] Compared with CH_4, CO_2 has stronger solubility in oil and has a better effect on reducing the oil viscosity and swelling the oil volume.[35] Some scholars have also found that a small amount of CH_4 can promote the oil swelling effect,[36,37] and the gas mixture has a more significant effect on improving the oil fluidity through experiments. However, under the nano "limited domain effect", fluid migration properties are strongly affected by mineral surface interactions, and the molecular arrangement between gas−liquid two phases is significantly different from that in conventional reservoirs.[38−40] Conventional experiments and numerical simulation methods make it difficult to accurately describe the interaction between the CO_2 and oil.

Molecular simulation is an effective method to explore the microstructure changes and interaction mechanisms at the molecular and atomic levels. By constructing mineral models corresponding to different reservoirs, such as sandstone, carbonate, organic kerogen, and inorganic clay minerals, it has been widely used to explore important mechanisms such as fluid adsorption, displacement, and migration under the micropore throat structure of reservoirs.[41−48] More and more scholars have revealed the micromechanism of CO_2 enhanced oil recovery and storage through molecular simulation.[49−51] By using molecular dynamics simulation methods, Chilukoti et al.[52] studied the structure and mass transport properties of different *n*-alkanes on quartz. Santo and Striolo groups[53,54] explored the competitive adsorption between CO_2 and alkanes in the nanopores and clarified the mechanism of CO_2 stripping alkanes. Liu et al.[55,56] studied the swelling mechanism of CO_2 on saturated alkanes and further explored the properties of the water−oil interface by supercritical CO_2 through molecular dynamics simulation. The results showed that the solubility of CO_2 in alkanes had a direct relationship to the oil swelling effect. The increase in pressure, the reduction in temperature, and the straight-chain structure of the alkanes are of benefit to the volume swelling of the CO_2−alkane systems. In the presence of a water phase, CO_2 preferred to display surface-active at the water−oil interface, and the interfacial tension between water−CO_2−decane decreased linearly with the increase of CO_2 concentration. Li et al.[57] studied the interface interaction between injected gas type and Bakken crude oil through molecular simulation methods. The results showed that compared with those of CO_2 and CH_4, ethane had the lowest minimum miscible pressure and the highest solubility in oil, and the effect on oil recovery was relatively best. Mohammed et al.[58] investigated the effect of supercritical CO_2 (Sc-CO_2) on the interfacial and transport properties of water−oil systems. It was found that the CO_2 film formed between the water and oil phases can displace the hydrocarbons from the interface. Sc-CO_2 can dilute the interface, form hydrogen bonds with water which stabilize the CO_2 film and reduce the interfacial tension in all systems. Wang et al.[59,60] explored the miscible behavior between CO_2 and oil in the nanoslit through molecular dynamic simulation. It was found that van der Waals interaction between oil and CO_2 was the main driving force for their miscibility, and it was more difficult for CO_2 to be miscible with polar oil because of the strong interaction between polar molecules and mineral surfaces. Dong et al.[61] constructed five kinds of porewall models and analyzed the effects of oil components, mineral types, and CO_2 concentration on oil replacement behavior. The results showed that the replacement efficiency increased with the increase of the CO_2 concentration in inorganic pores, while in organic pores, the CO_2 concentration mainly affected the replacement efficiency of light oil but had no obvious effect on heavy oil. Comparing the miscible behavior between CO_2 and oil in the bulk phase and nanoslit, Fang[62] concluded that tight reservoirs with micropores are more likely to make CO_2 and oil miscible. To sum up, currently, most studies mainly focus on the changes in the properties of the oil−gas interface in the bulk phase or nanoslit, without considering the influence of mineral surface and fluid adsorption on the oil−gas interface. There is still a lack of a systematic and comprehensive comparative analysis of the miscibility characteristics between CO_2 and oil.

In this work, based on the total hydrocarbon analysis results of tight oil samples in Block H of Yanchang Oilfield, *n*-octane, *n*-dodecane, and *n*-eicosane were selected to represent the light, medium, and heavy component oil, respectively. The effects of four factors on the microscopic mechanism of CO_2 and oil miscibility were studied by a molecular dynamics simulation. First, the CO_2−oil miscible model was constructed, and the simulation methods were explained. Second, the microscopic miscibility characteristics of CO_2 and different component oil under reservoir conditions of 320 K and 15 MPa were discussed. Finally, the effects of formation pressure, temperature, and CH_4 content on the miscibility of CO_2−oil were clarified in detail by analyzing the solubility, diffusion coefficient, interaction energy, and other parameters. The study results systematically reveal the microscopic mechanism of the effect of CO_2 on the oil miscibility characteristics and have significant theoretical guidance for improving CO_2 flooding in tight sandstone reservoirs.

2. MODEL AND METHODS

2.1. Molecular Models. The model can be divided into three regions, including the sandstone mineral surface, the fluid phase, and the virtual baffle, preventing CO_2 molecules from escaping the system. The surface of sandstone minerals is characterized by completely hydroxylated α-quartz.[61]

The construction process of the three-dimensional periodic molecular model of CO_2 and oil miscibility was constructed as follows: (1) α-SiO_2 crystals were derived from the simulation

https://doi.org/10.1021/acsomega.4c00541
ACS Omega 2024, 9, 15663−15676

library of Materials Studio software and cut along the (1 0 0) plane to obtain a stable crystal structure. Hydroxylated silica was obtained by hydrogenation on the unbonded oxygen atoms in the crystal, and then a quartz surface of 5.4 × 5.4 × 9.88 nm was obtained by expanding the crystal cell. (2) The system pressure was determined by fluid density, and the length and width of the oil layer and CO_2 solvent layer under different pressures were consistent with the quartz surface. The height of the oil layer was 2.57 nm, and the height of the CO_2 solvent layer was 4.09 nm. According to the purpose of the study, oil and CO_2 densities were set under different temperature and pressure conditions with reference to the data published by the National Institute of Standards and Technology (NIST)[63] and the AP1700 physical property platform.[64] (3) The constructed simulated oil layer was spliced with the quartz surface. In order to obtain the initial equilibrium adsorption configuration of the oil film, the 2 ns dynamic equilibrium calculation of the oil layer was carried out on the quartz surface first. Then, the CO_2 solvent layer was placed on the oil film, and the virtual baffles were added above to maintain the pressure balance of the system. (4) Finally, an 8 nm vacuum layer was added above the model to avoid the influence of periodic boundary conditions. The initial configuration of the three-dimensional periodic simulation of the CO_2 and oil miscibility is shown in Figure 1.

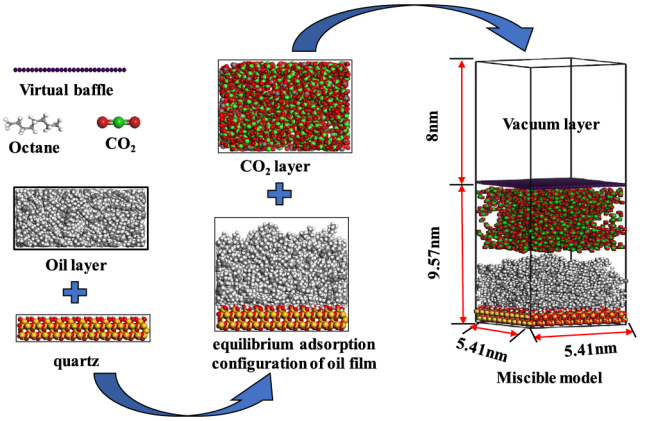

Figure 1. Model structure.

2.2. Simulation Details. In this study, all interatomic interactions were described using the force field of Condensed-Phase-Optimized Molecular Potential for Atomistic Simulation Studies (COMPASSIII), a widely used whole-atom force field optimized based on ab initio and experimental data, which has been proven to accurately predict the structure and thermophysical properties of organic and inorganic substances.[65] The force field mainly includes bonding energy and nonbonding energy. Bonding energy generally includes bond stretching energy E_{bonds}, bond angle bending energy E_{angles}, bond torsion energy $E_{dihedrals}$, bond angle out of plane bending energy $E_{impropers}$, and mutual coupling energy E_{cross}. While nonbonding energy $E_{nonbonded}$ includes van der Waals energy E_{vdw} and Coulomb electrostatic energy E_{ele}. The total potential energy equation is expressed as follows:[66]

$$E = E_{bond} + E_{angle} + E_{dihedral} + E_{cross} + E_{nonbonded} \quad (1)$$

The expressions of nonbonding energy in the COMPASSIII force field are as follows:

$$E_{vdw} = D_0\left[2\left(\frac{R_0}{R}\right)^9 - 3\left(\frac{R_0}{R}\right)^6\right] \quad (2)$$

$$E_{ele} = C\frac{q_i q_j}{\varepsilon R} \quad (3)$$

where D_0 is the depth of the potential well, R_0 is the Lennard−Jones radius, R is the distance between atoms, C = 332.0647(kcal/mol)Å/e^2 is the conversion factor, q_i and q_j are the electrostatic charge of atom i and atom j, respectively, and ε is the relative dielectric constant.

All simulations in this article were performed using the Materials Studio 2023 software package for molecular dynamics calculations. In the process of molecular simulation, the quartz surface and virtual baffle were fixed first. The atomic coordinates were iteratively calculated by using the Smart method to prevent extreme potential energy values between particles from causing system operation failure. After geometric optimization, the initial reasonable configuration of the system was obtained. Then, the dynamics simulation was carried out under the NVT ensemble (constant of atomic number, system volume, and temperature). The corresponding temperature was set according to the research content and was controlled

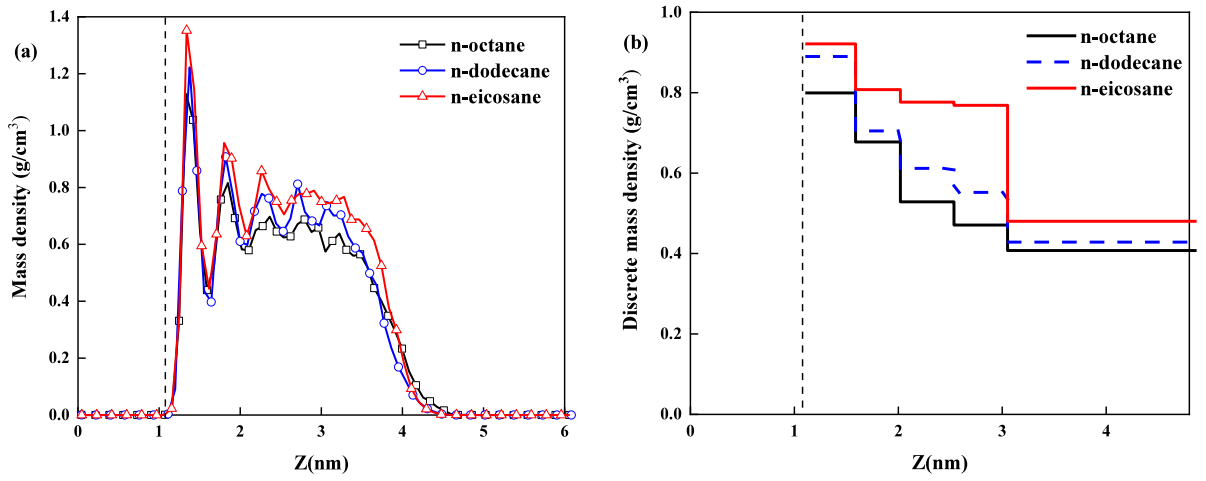

Figure 2. Continuous (a) and discrete (b) mass density distributions of different component oil along the Z direction.

https://doi.org/10.1021/acsomega.4c00541
ACS Omega 2024, 9, 15663−15676

by the Nose−Hoover algorithm. The remote electrostatic interaction was calculated by using the Ewald summation algorithm. The van der Waals interaction was calculated using an atomic summation algorithm, and the truncation radius was set to 12.5 Å. The time step was 1 fs, and data were recorded every 1000 steps for analysis. The equilibrium state of the system was ensured by checking the temperature, pressure, energy, and other parameters.

3. RESULTS AND DISCUSSION

3.1. Microscopic Miscible Characteristics and Mechanisms of CO_2−Oil. To compare the miscibility between

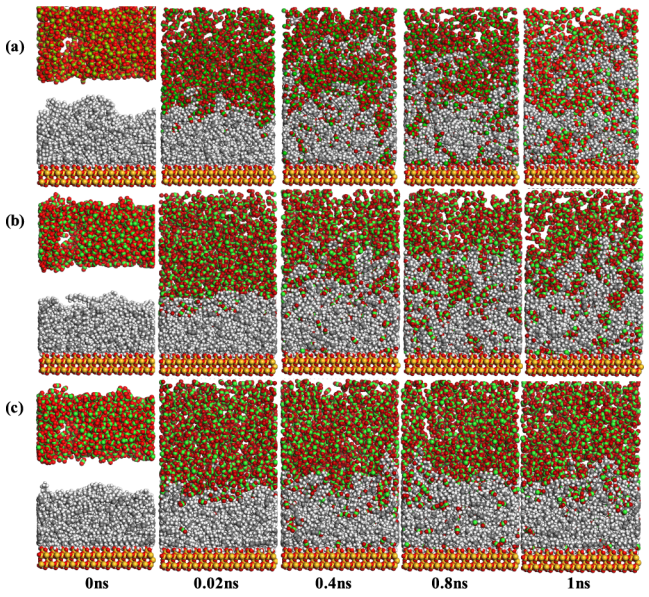

Figure 3. Miscible process of CO_2 and oil: (a) light component system, (b) medium component system, and (c) heavy component system.

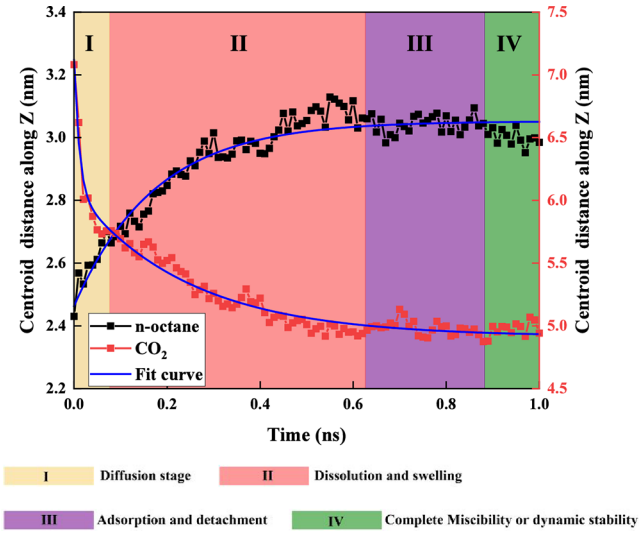

Figure 4. Centroid displacement curves of *n*-octane and CO_2 during dynamic equilibrium.

CO_2 and different oil components , the adsorption properties of *n*-octane, *n*-dodecane, and *n*-eicosane on the quartz surface were studied. Molecular dynamics simulation can only get

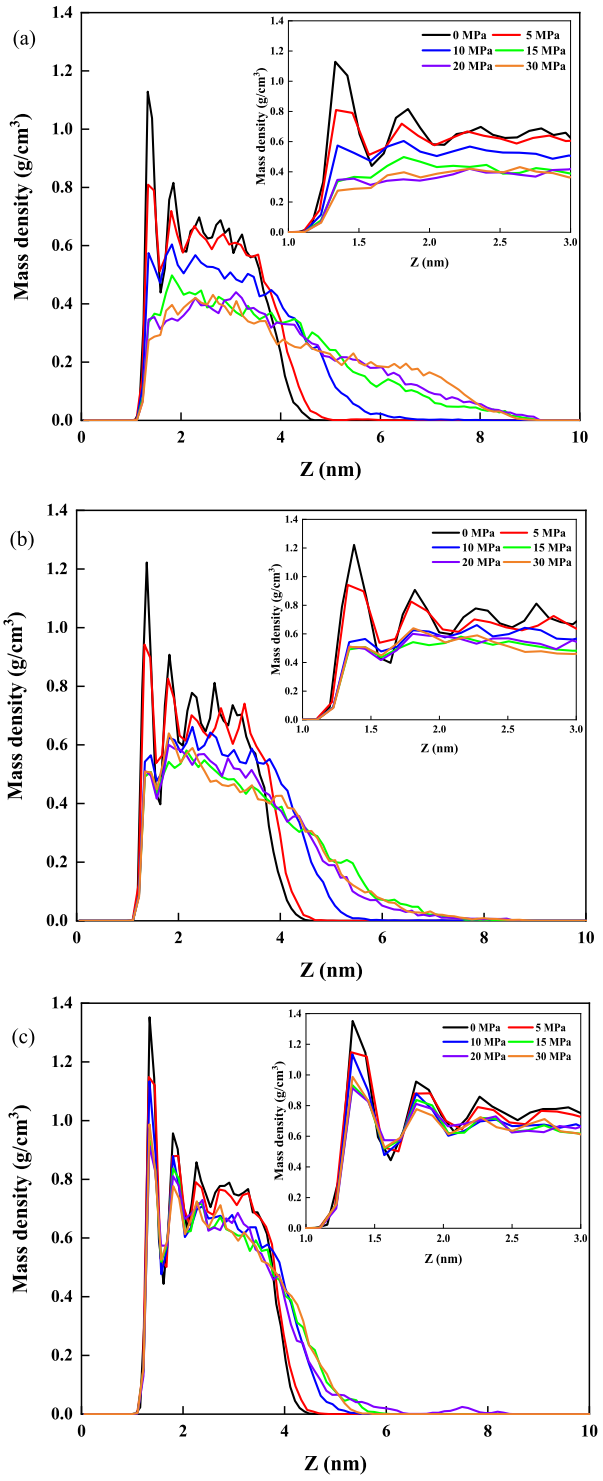

Figure 5. Oil density distribution under different pressures: (a) *n*-octane, (b) *n*-dodecane, and (c) *n*-eicosane.

microscopic information about individual molecular trajectories, so it needs to be converted into the necessary macroscopic properties for data analysis through statistical thermodynamics. Therefore, the simulation system must be divided into N_b bins along the Z direction to obtain the fluid density distribution. The volume of each bin is $L_x \times L_y \times (H_{eff}/N_b)$. The flag function $H_n(Z_i)$ is defined as[67]

https://doi.org/10.1021/acsomega.4c00541
ACS Omega 2024, 9, 15663−15676

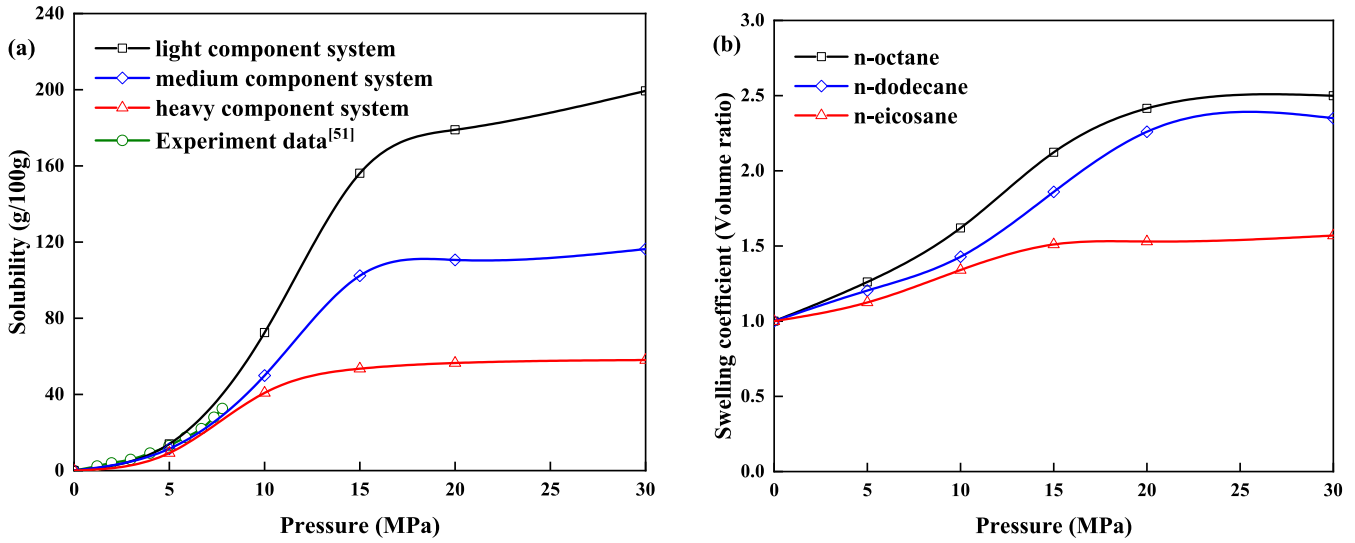

Figure 6. Influence of pressure on the CO_2 solubility (a) and oil swelling coefficient (b).

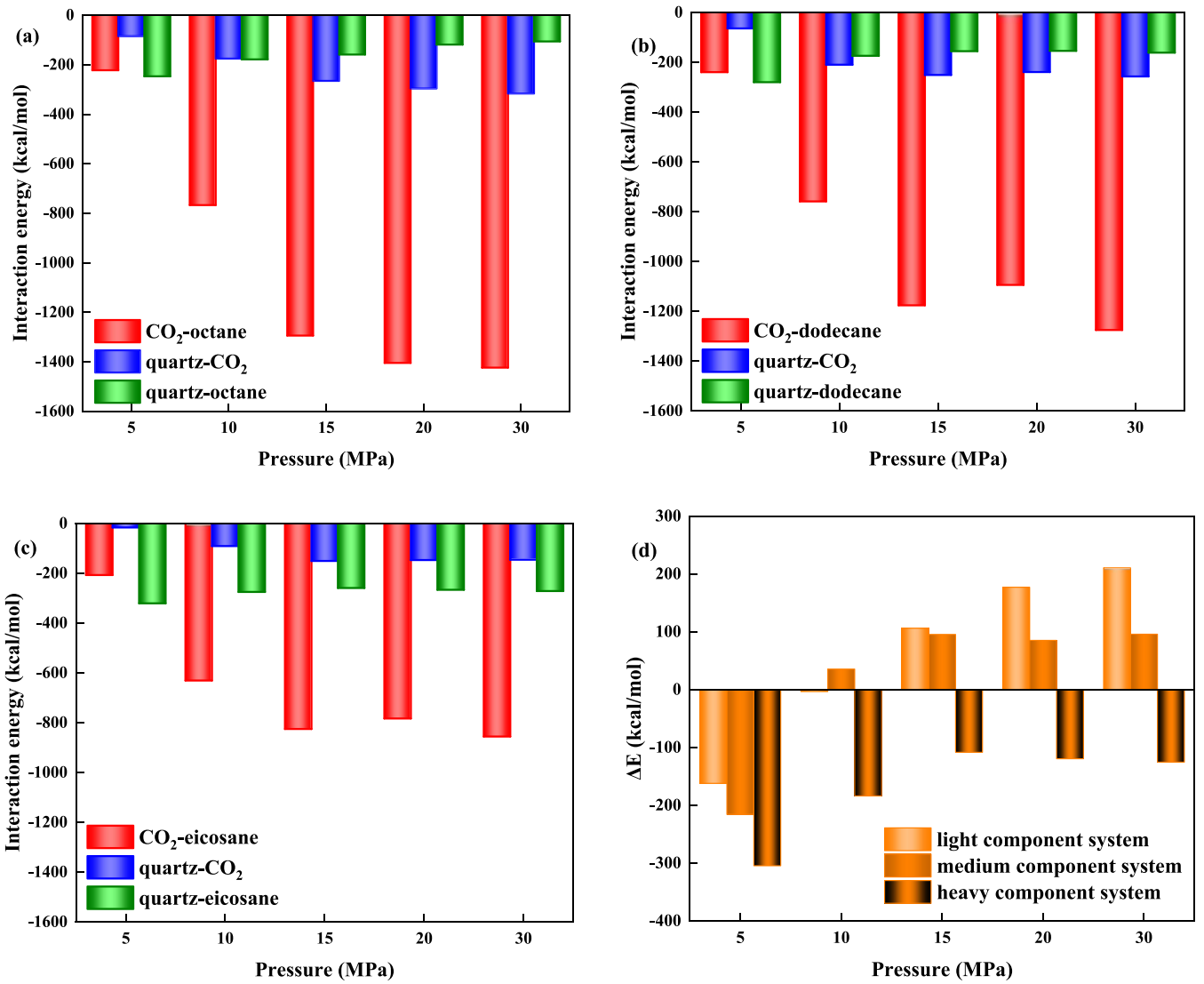

Figure 7. Variation of interaction energy: (a) light component system, (b) medium component system, (c) heavy component system, and (d) difference of interaction energy between quartz−oil and quartz−CO_2.

https://doi.org/10.1021/acsomega.4c00541
ACS Omega 2024, 9, 15663−15676

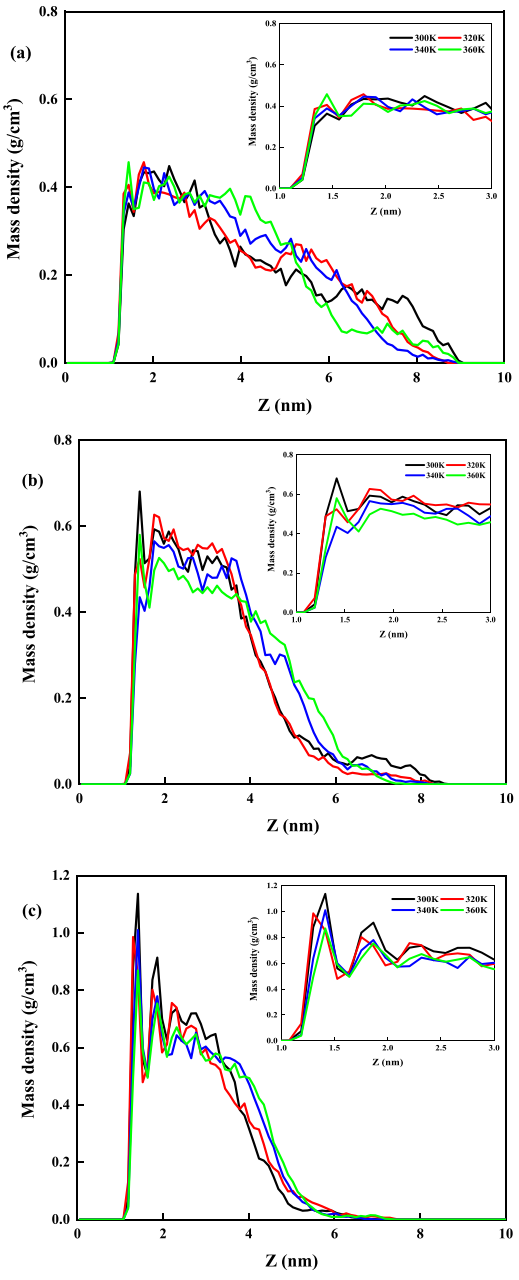

Figure 8. Oil density distribution at different temperatures: (a) *n*-octane, (b) *n*-dodecane, and (c) *n*-eicosane.

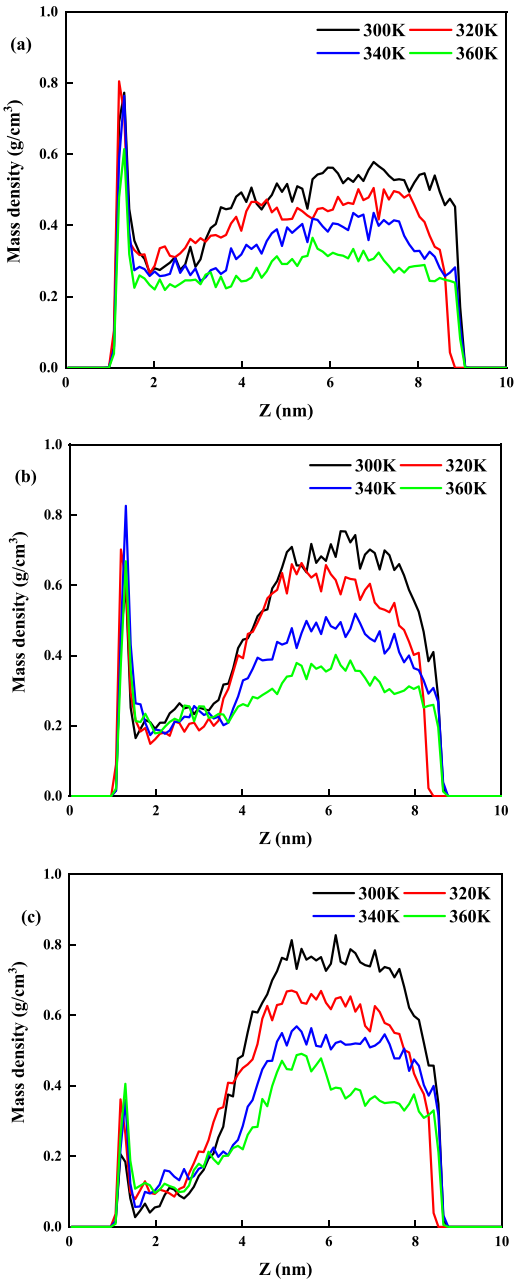

Figure 9. Density distribution of CO_2 with temperature change in different systems: (a) light component system, (b) medium component system, and (c) heavy component system.

$$\begin{cases} H_n(z_{i,j}) = 1 & (n-1)\Delta z < z_i < n\Delta z) \\ H_n(z_{i,j}) = 0 & (\text{otherwise}) \end{cases} \tag{4}$$

Then, from time step J_N to J_M, the mean number density ρ_{number} and local mass density ρ_{mass} of the n-th bin are

$$\rho_{number} = \frac{1}{A\Delta z(J_M - J_N + 1)} \sum_{J=J_N}^{J_M} \sum_{i=1}^{N} H_n(z_{i,j}) \tag{5}$$

$$\rho_{mass} = \frac{10^{21}}{N_A} \frac{1}{A\Delta z(J_M - J_N + 1)} \sum_{J=J_N}^{J_M} \sum_{i=1}^{N} H_n(z_{i,j}) M_i \tag{6}$$

The mass density distribution profiles of different oil components on the quartz surface are shown in Figure 2. It is found that the three kinds of component oil form several prominent adsorption peaks on the quartz surface, respectively. The positions of the adsorption peaks are almost the same, but the values are quite different. The oil molecular chains convolve and aggregate with each other, and finally adsorb on the quartz in an orderly and stable manner. As the distance increases, the interaction between the oil and quartz weakens, leading to a gradual decrease the oil density. The first adsorption layer densities of *n*-octane, *n*-dodecane, and *n*-eicosane are 0.79 g/cm^3, 0.88 g/cm^3, and 0.92 g/cm^3, respectively. Compared with the first adsorption layer and the initial oil density (0.67 g/cm^3, 0.72 g/cm^3, and 0.8 g/cm^3), it can be seen that the oil density near the quartz surface is about 1.2 times that of the initial density, indicating that the interaction between mineral surfaces and fluid has a significant

https://doi.org/10.1021/acsomega.4c00541
ACS Omega 2024, 9, 15663−15676

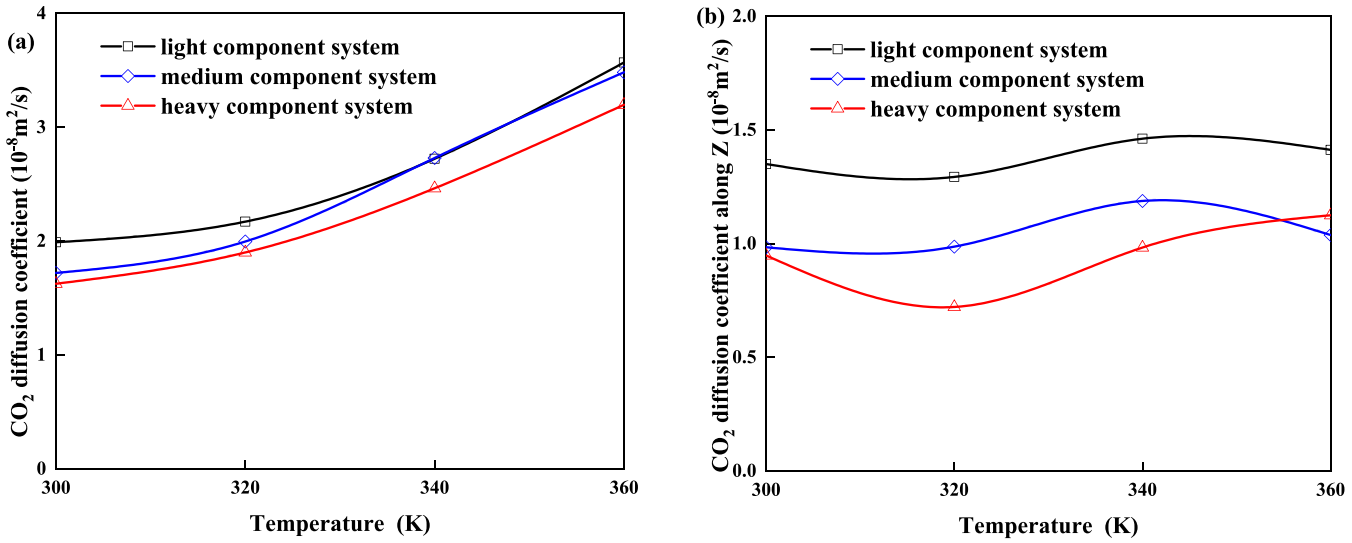

Figure 10. Total diffusion coefficient of CO_2 in different systems (a) and the CO_2 diffusion coefficient in the vertical surface along the Z direction (b).

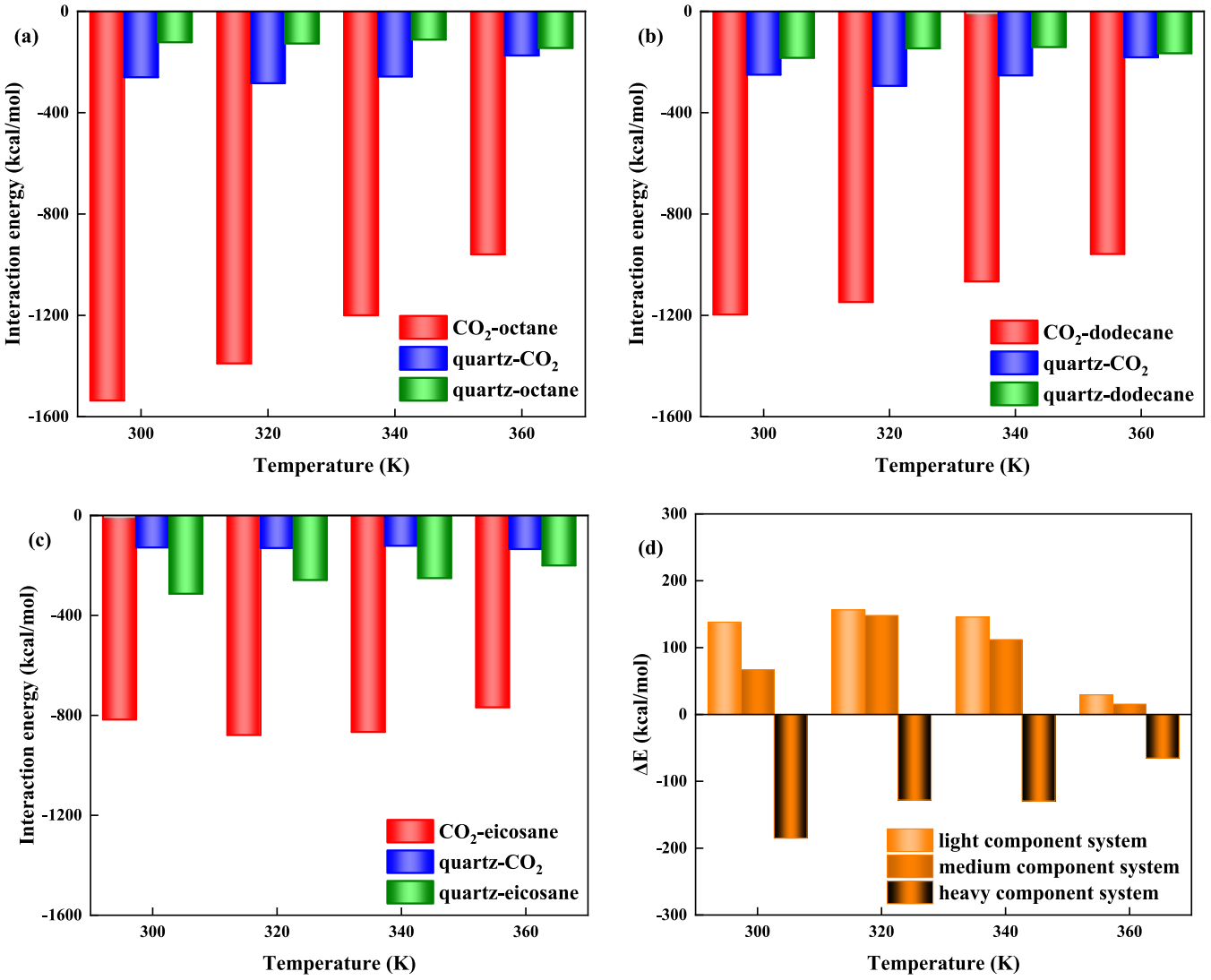

Figure 11. Variation of interaction energy: (a) light component system, (b) medium component system, (c) heavy component system, and (d) difference of interaction energy between quartz−oil and quartz−CO_2.

https://doi.org/10.1021/acsomega.4c00541
ACS Omega 2024, 9, 15663−15676

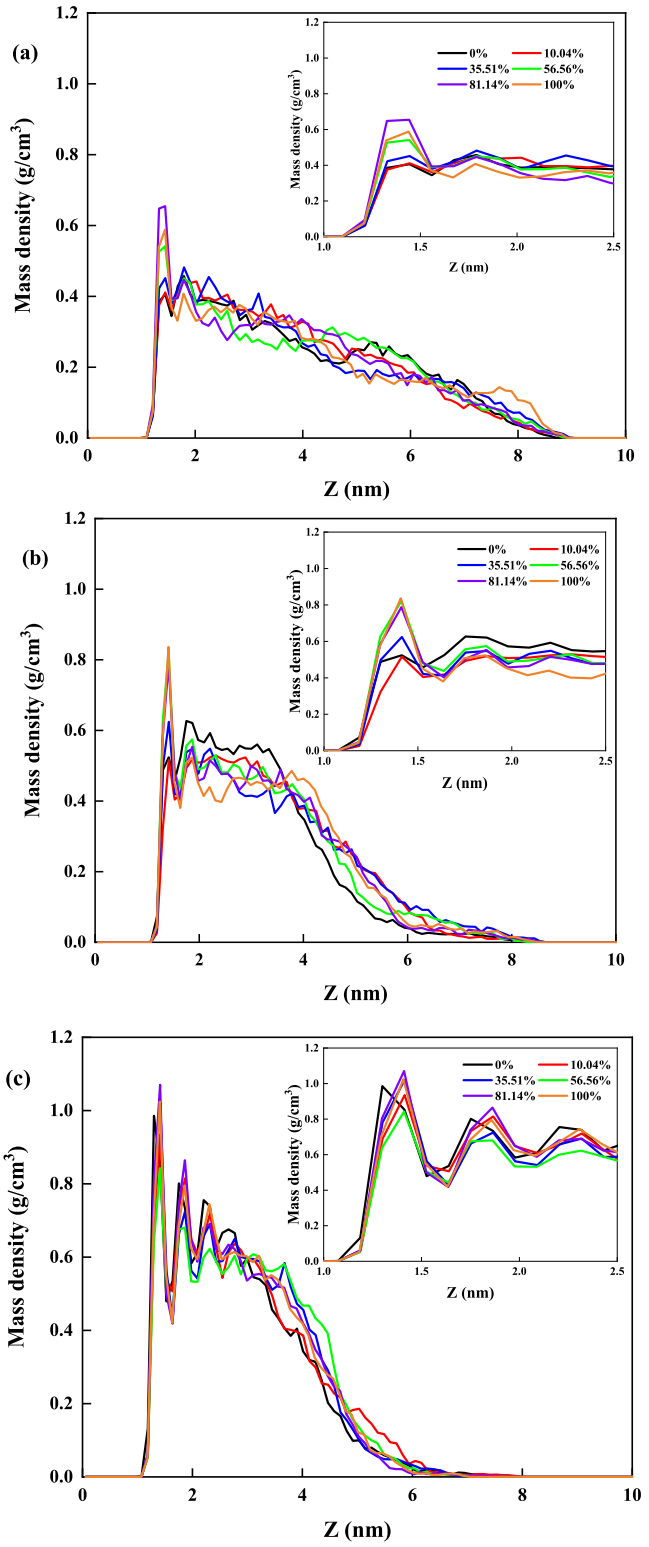

Figure 12. Oil density distribution with different CH_4 contents: (a) *n*-octane, (b) *n*-dodecane, and (c) *n*-eicosane.

impact on the occurrence of oil in tight sandstone reservoirs, and the intermolecular interaction cannot be ignored.

Figure 3 shows a series of processes of dynamic miscibility of CO_2 and *n*-octane, *n*-dodecane, and *n*-eicosane at 320 K and 15 MPa reservoir conditions. Under the strong diffusion effect of CO_2 molecules, it rapidly diffuses to the oil interface within 0.2 ns from the beginning of the simulation. Due to the differences in oil components, the microstructure of the oil–gas two-phase interface shows different changes over time. For light component oil, with the increase of the interaction between CO_2 and oil, the alkane chains are fully stretched, and the system's dispersion is enhanced. As the oil molecules escape from the constraint of the oil film to the CO_2 phase, the oil–gas interface gradually weakens. When a large number of CO_2 molecules penetrate the oil film to adsorb on the quartz, the oil film is effectively detached. Finally, CO_2 and oil achieved complete miscibility. For medium component oil, the miscibility process is similar to that of the light component system. CO_2 can effectively improve oil fluidity and promote oil swelling. But, because the molecular weight of oil in the medium component system is relatively large, the miscibility of CO_2 and oil is weaker than that of the light component system at the same time. For heavy component oil, oil molecules are more inclined to self-agglomerate and closely adsorb on the quartz. Only a few *n*-eicosane alkanes dissolve and diffuse into the CO_2 fluid phase, and the interface structure of the two phases does not change much with an increase in simulation time. After simulation, there is still an obvious oil–gas interface between CO_2 and oil.

The centroid distribution of *n*-octane and CO_2 during the dynamic simulation was analyzed in detail to clarify the microscopic interaction mechanism of the two phases on quartz during the miscible process. The miscible process can be divided into four stages, as shown in Figure 4. (1) Rapid diffusion stage: the effect of CO_2 diffusion plays a significant role, and CO_2 quickly migrates to the oil interface. (2) CO_2 dissolution and oil swelling stage: the two-phase interface changes from flat to rough with the dissolution of CO_2 in oil. The alkane molecules are further stretched, and the oil phase volume increases, corresponding to the CO_2 swelling effect on a macro level. While the previous process is ongoing, the void between oil molecules also increases, providing favorable conditions for forming advantageous diffusion channels for CO_2. (3) Competitive adsorption and oil film detachment stage: after forming the advantageous diffusion channel, CO_2 competitively adsorbs with oil molecules by occupying the adsorption site of alkane molecules on the mineral surface. It weakens the interaction between oil and quartz, finally making the oil film detached effectively. (4) Miscible or dynamic equilibrium stability stage: for light or medium component oil, CO_2 can be fully miscible with the oil phase, and the fluid phase interface disappears to reach the completely miscible or nearly miscible phase. Whereas, for heavy component oil, the alkane molecule has a large self-cohesion and is more inclined to self-agglomerate to keep the thick-layer oil film firmly adsorbed on the quartz. CO_2 has a limited effect on the dissolution and swelling of the heavy oil. As a result, they can reach only a dynamic equilibrium and stability stage.

3.2. Effect of Pressure on Miscibility Characteristics.

In the process of CO_2 injection and flooding, the formation pressure gradually decreases from the injection site to the production site. The fluid phase changes greatly with the increased distance of the CO_2 migration, leading to a change in the interaction mechanism between the two phases of oil and gas. Therefore, it is necessary to explore the influence of the pressure on the miscibility of CO_2 and oil. Based on the reservoir temperature 320 K in Block H of Yanchang Oilfield, a series of pressure values of 5, 10, 15, 20, and 30 MPa were set. Then, the simulation results were compared with those of the CO_2 pressure condition of 0 MPa.

https://doi.org/10.1021/acsomega.4c00541
ACS Omega 2024, 9, 15663–15676

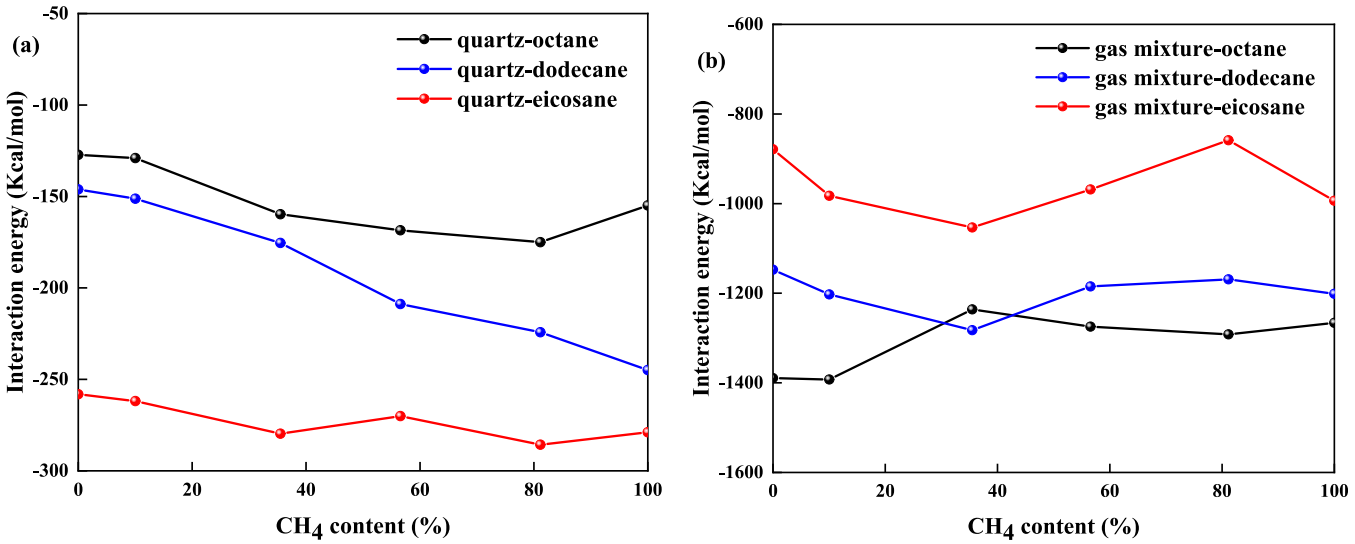

Figure 13. Variation of the interaction energy in different systems with CH_4 content: (a) quartz−oil and (b) gas mixture−oil.

Figure 5 shows the density distribution of oil molecules along the *Z* axis after sufficient interaction of CO_2 with oil under different pressure systems. It can be seen that the oil density significantly decreases compared to the adsorption density curve without CO_2, illustrating that the addition of CO_2 breaks the structure of the initial aggregation state between the oil molecules. When the pressure is 5 MPa, although the density of different oil components decreases relative to the initial data, the first adsorption peak is still clearly visible. Meanwhile, the oil volume does not increase from the density distribution range. Under low pressure, CO_2 can disturb only the oil far from the quartz through the diffusion effects. The short-range van der Waals interaction between the alkane chains causes the oil molecules on the quartz to stretch out, so the peak density distribution is slightly reduced. However, the oil volume is almost unchanged. When the pressure is greater than 10 MPa, CO_2 is in a supercritical state, which has both the density of the liquid and the viscosity of the gas and has good fluidity, super solubility, strong diffusion, and mass transfer. Except for the heavy component oil system, the higher the pressure, the smaller the peak values of the density distribution of oil and the wider the oil distribution range. For light and medium component oil systems, the adsorption peaks almost disappear when the pressure is 15 MPa, and the maximum density of oil near the quartz is about 0.43 g/cm^3 and 0.52 g/cm^3, which are 38.05% and 42.62% of the maximum adsorption oil density of initial configuration. The results show that CO_2 has strong miscibility (swelling and detaching effect), which can effectively displace the light and medium oil adsorbed on quartz by increasing the CO_2 pressure. For the heavy component oil system, it can be seen that no matter how much the CO_2 pressure is increased, the oil adsorption peaks still exist, and the oil distribution range is almost unchanged. Although the pressure is 30 MPa, the oil molecular is still "firmly" adsorbed on the mineral surface. The maximum density of the first adsorption peak is 0.97 g/cm^3, much higher than the initial oil density of 0.814 g/cm^3. That shows it is difficult to remove it from the mineral surface only by the static swelling effect of CO_2.

Figure 6 shows the solubility and swelling coefficient between CO_2 and different oil components. *Solubility* is defined as the mass of dissolved CO_2 per 100g of oil in g/100g. The *swelling coefficient* is defined as the oil volume ratio of the thoroughly mixed oil and gas to the initial. Under constant mass conditions, it can also be calculated by the ratio of the initial oil density to the oil density after gas dissolution. To verify the reliability of the simulation results, the CO_2 solubility in the simulated medium component system was compared with the experiment data.[68] It can be seen from Figure 6a that the two have high coincidence, and the error sources mainly include the settings of the simulation system and the selection of force field parameters. The accuracy of our simulation results and the prediction of relevant properties under high temperature and pressure conditions are not affected, which is also confirmed by relevant studies.[69] The solubility is not only related to the system pressure but also closely related to the oil composition. When the pressure is less than 5 MPa, where CO_2 is the gas phase, the solubility in different oil systems is small. There is no apparent difference in the solubility. When the pressure is greater than 10 MPa, where CO_2 is in a supercritical state, the solubility decreases with the increase in oil molecular weight. The solubility first increases and then becomes stable with an increase in pressure. For light component oil, the CO_2 solubility increases from 72.47g/100g to 199.42g/100g when the pressure rises from 10 to 30 MPa. For heavy component oil, it is more likely to self-entanglement and agglomerate under the interaction of van der Waals. Even if the CO_2 pressure increases, it is difficult to effectively disturb the internal oil molecules, which dramatically reduces the contact area between CO_2 and alkanes. After the pressure exceeds 15 MPa, the CO_2 solubility hardly changes with the increase in pressure. As can be seen from Figure 6b, the change in the oil swelling coefficient is consistent with the trend of the CO_2 solubility, indicating that the oil swelling capacity is directly related to the CO_2 solubility. Some scholars concluded that there was also an excellent linear relationship between the solubility and swelling coefficient.[70,71] In different systems, the swelling coefficient increases with the increase of CO_2 pressure and decreases with the increase of the oil molecule's weight. Under the supercritical state, the miscibility of CO_2 with light and medium component oil changes more obviously as the pressure increases. Generally speaking, the more excellent the

https://doi.org/10.1021/acsomega.4c00541
ACS Omega 2024, 9, 15663−15676

solubility of CO_2, the stronger the swelling capacity of oil, and the better the effect of CO_2 displacing oil.

The balance relation of the interaction energy between each component determines its different migration behaviors. Figure 7 shows the interaction energies between CO_2−oil, quartz−oil, and quartz−CO_2, and the differences between quartz−oil and quartz−CO_2 under different pressures. The interaction energy is defined as

$$E_{\text{quartz-oil}} = E_{\text{total}} - (E_{\text{quartz}} + E_{\text{oil}}) \quad (7)$$

where, $E_{\text{quartz-oil}}$ is the interaction energy between the quartz and the oil molecules, E_{total} is the total interaction energy between the two, and E_{quartz} and E_{oil} are the single point energy of the quartz and oil molecules, respectively. The interaction energy between the CO_2−oil and quartz−CO_2 can be obtained by the same methods.

It can be seen from Figure 7a−c that the interaction energy between CO_2 and oil molecules increases with the increase of pressure. In contrast, the interaction energy between quartz and oil molecules decreases. That indicates that the increase of the CO_2 pressure weakens the adsorbing ability of the quartz to oil molecules, increases the contact area between CO_2 and the oil system, and enhances the effect of CO_2 on dissolution and oil swelling. When the pressure is 5 MPa, the adsorption energy of oil on the quartz is much higher than that of CO_2, and the interaction energy between CO_2 and different oil components is no obvious distinction. When the pressure is greater than 10 MPa for light and medium component systems, the interaction energy of CO_2 on the quartz is greater than that of oil. The oil molecules adsorbed on the quartz can be gradually replaced by CO_2 in this pressure range, which explains that CO_2 can effectively detach the oil film on the mineral surface only when the pressure reaches a specific value. For the heavy component system, the interaction energy between CO_2 and *n*-eicosane is much smaller than those of the light and medium component systems. The interaction energy of *n*-eicosane on quartz does not change much with the increase in pressure, and the interaction between the quartz and CO_2 is small. Therefore, the dissolution and swelling effect of CO_2 on the heavy component oil is poor.

Figure 7d directly shows the difference in the interaction energy between quartz−oil and quartz−CO_2 under different pressure conditions. Negative values indicate that the adsorption energy of oil on quartz is greater than that on CO_2. The greater the absolute value of ΔE, the stronger the adsorption effect of oil on quartz, and the weaker the miscibility of CO_2 to oil. In contrast, the positive value indicates that the adsorption energy of the quartz on oil is less than that of CO_2. The greater the absolute value of ΔE, the weaker the adsorption effect of oil on the quartz, the stronger the miscibility of CO_2 to oil, and the better the displacement effect on oil. It can be seen that with the increase of pressure, the ΔE presents a gradual increase trend in the light component system, and the ΔE increases first and then tends to be stable in the medium component system, indicating that CO_2 has the strongest miscibility and the best displacement effect on light component oil. Although the ΔE is increased in the heavy component system, it is still negative, indicating that the adsorption energy of heavy component oil on the quartz is much higher than the dissolution and swelling energy of CO_2 on oil molecules. Increasing the CO_2 pressure to improve the static swelling effects makes it difficult to displace the heavy component oil from the quartz. It also reveals the mechanism of the CO_2 extraction of the light component oil, but it is difficult to replace the heavy component oil.

3.3. Effect of Temperature on Miscibility Characteristics. The influence of temperature on the miscibility mechanism of CO_2 and oil is relatively complex, which is mainly reflected in two aspects: (1) the increase in temperature will reduce the oil viscosity, increase the oil fluidity, and increase the CO_2 diffusion coefficient to promote the oil swelling. (2) Rising temperature will reduce the CO_2 density and the solubility, which is not beneficial for the CO_2−oil miscibility. It is significant to explicitly evaluate the effect of temperature on the miscibility of CO_2 and oil to evaluate CO_2 flooding. Under the condition of system pressure of 15 MPa, a series of temperature values of 300, 320, 340, and 360 K were set to explore the influence of temperature on the miscibility characteristics of CO_2 and oil.

Figure 8 shows the oil density distribution on quartz at different temperatures. As seen from Figure 8a, in the light component system, the *n*-octane density at the first adsorption peak is significantly lower than that in the free volume zone when the temperature is less than 340 K. The *n*-octane density decreases linearly and slowly with the increase in the *Z* direction distance. The distribution range is almost full of the entire confined zone, indicating that CO_2 has a strong miscibility to oil and can effectively detach the oil film. When the temperature rises to 360 K, the *n*-octane density of the first adsorption peak increases and the ability of CO_2 to replace oil is slightly weakened. Overall, under the condition of 15 MPa, there is little difference in temperature on the miscibility of CO_2 and oil in the light component system. It can be seen in Figure 8b that an appropriate increase in temperature is conducive to reducing the adsorption interaction of *n*-dodecane on the quartz. The *n*-dodecane density peak value of the first layer is the smallest at 340 K, and the peak distribution range is the widest. However, when the temperature rises to 360 K, the *n*-dodecane density adsorbed on the quartz increases instead of decreasing. It can be seen that there is a critical temperature at which CO_2 has the strongest miscibility to oil. For the heavy component system, although the *n*-eicosane adsorption density decreases with an increase in temperature, three adsorption peaks are still clearly visible, as can be seen in Figure 8c.

Taking CO_2 as the research object, we calculated the CO_2 density and diffusion coefficient in different systems. As can be seen in Figure 9, the CO_2 density far from the quartz decreases with an increase in temperature. However, the change of the CO_2 density in different systems near the quartz varies with temperature, mainly related to the competitive adsorption intensity between CO_2 and oil. For light and heavy component systems, the density of the CO_2 adsorbed phase near the quartz is higher than that far from the quartz. CO_2 can "disturb and evacuate" the aggregated and entangled oil molecules to form a gas phase flow channel and compete with the oil molecules for adsorption, thus effectively detaching the oil film attached to the quartz. When the temperature is 320 or 340 K, the CO_2 density of the adsorbed phase can reach the maximum, and the effect on oil detachment is the best, corresponding to the results of the oil density distribution analysis above. For the heavy component oil system, the CO_2 density in the first adsorption layer is much lower than that in the free volume zone, which indicates that CO_2 can only diffuse in the free volume zone, and it is difficult to break through the high

https://doi.org/10.1021/acsomega.4c00541
ACS Omega 2024, 9, 15663−15676

intermolecular cohesion energy of oil molecules in the system to replace oil effectively.

To quantitatively characterize the miscible effect of CO_2−oil, the CO_2 diffusion coefficients in the whole system and on the vertical quartz surface along the Z direction were calculated. It can be seen from Figure 10a that with the increase in temperature, the average motion energy of gas molecules increases and the CO_2 diffusion coefficient in the miscible system increases exponentially. However, from the perspective of the Z direction perpendicular to the quartz (Figure 10b), the CO_2 diffusion coefficient does not continue to rise because of the adsorption interaction of oil and the quartz surface. The smaller the mass of oil components, the stronger the diffusion ability of CO_2 in the system, and the better the effect on oil replacement. At 340 K, the CO_2 diffusion coefficient in the Z direction of the light and medium component systems is the highest, the CO_2 concentration in the adsorbed phase is also relatively the highest, and the oil density near the quartz is relatively the lowest, indicating that the miscibility of CO_2 and oil is relatively the best at this temperature. For the heavy component system, the CO_2 diffusion coefficient along the Z direction first decreases and then increases with the increase in temperature, which is good for promoting the miscibility of CO_2 and heavy oil.

As shown in Figure 11a−c, the interaction energy between CO_2 and oil in the light component system is the highest under the same conditions, and the miscibility effect is the best. When the pressure and volume of the system are constant, the CO_2 density decreases with the increase in temperature, leading to a decrease in the interaction energy between CO_2 and oil. Notably, in the heavy component system, within a specific temperature range, the interaction energy between CO_2 and oil increases with temperature, and the interaction energy between quartz and oil decreases with the increase in temperature. However, the interaction energy between quartz and CO_2 hardly changes. That indicates that CO_2 cannot penetrate the heavy component oil molecules to adsorb on the quartz, but increasing the temperature can effectively improve the fluidity of heavy oil components and weaken the adsorption effect on the quartz. It indicates that an increase in temperature in a specific range is conducive to improving the contact area between CO_2 and oil and promoting the interaction. Figure 11d shows the differences in interaction energy between quartz−oil and quartz−CO_2 under different temperature conditions. The results show that in the light and medium component oil systems, the ΔE is positive with the temperature increase and shows a trend of first increasing and then decreasing. It shows that there is a critical temperature, which makes the miscibility of CO_2 to light and medium oil the strongest, and the effect of oil replacement is the best. For the heavy component system, with the increase in temperature, the interaction energy between quartz and oil is greater than that between quartz and CO_2, and the miscibility between CO_2 and heavy component oil is poor.

3.4. Effect of CH_4 Content on Miscibility Characteristics. At the same volume, the total number of gas molecules in the system was maintained constant, and the mass content of CH_4 was set to 0%, 10.04%, 35.5%, 56.56%, 81.14%, and 100%, respectively.

Figure 12 shows the effect of the CH_4 content on the oil density. When the CH_4 content in the light component system is greater than 35.5%, the first adsorption peak value of *n*-octane density increases significantly, but the distribution range is almost unchanged, indicating that the increase of CH_4 content weakens the detachment effect of CO_2 on the adsorbed oil, and the gas mixture still has a good dissolution and swelling effect on the light component system. For the medium component system, when the CH_4 content is less than 10.04%, there is no prominent adsorption peak in the *n*-dodecane density distribution curve. Compared with pure CO_2, which means the CH_4 content is 0%, the dodecane density of the free volume zone is relatively lower, and the distribution range is relatively extensive. When the CH_4 content is greater than 10.04%, the first adsorption peak value increases with the CH_4 content, and the oil density of the free volume zone decreases slightly. It shows that the increase of CH_4 can make the alkanes at the oil−gas interface looser under the disturbance of gas molecules and weaken the agglomeration effect between the alkane chains far from the quartz but is not helpful for the oil film detachment. For the heavy component system, the *n*-eicosane density distribution range in the mixture of CO_2 and CH_4 is relatively more extensive. When the CH_4 content is 56.56%, the oil density is relatively minimal, which indicates that a specific content of CH_4 can weaken the oil interaction intensity and promote oil swelling at the oil−gas interface.

Similarly, the interaction energy between quartz−oil and gas mixture−oil was calculated (Figure 13). It can be seen that with the increase of CH_4 content, the interaction energy of oil on the quartz gradually increases, which is not beneficial for oil film detachment. With the increase in molecular weight of alkanes, the interaction energy of oil−quartz increases and the interaction energy of oil−gas mixture decreases, which is not conducive to the miscibility. For the light component system, the interaction energy between the gas mixture and oil decreases first and then increases slightly with the increase in CH_4 content. In contrast to the trend of the light component system, the interaction between the gas mixture and oil can first increase and then decrease with an increase in CH_4 content in medium and heavy component oil systems. Adding an appropriate amount of the CH_4 mixture to CO_2 can increase the intensity of the gas mixture−oil interaction, increase the fractional free volume between the alkane chains, and further promote the oil swelling effect far from the quartz. Therefore, the appropriate CH_4 content is conducive to the miscibility of CO_2 and oil. If the CH_4 content is excessive, then the interaction between the gas mixture and oil can be reduced, and the oil cannot be effectively replaced.

4. CONCLUSIONS

In this work, we systematically explored the effects of oil composition, formation pressure, temperature, and CH_4 content on the miscible mechanisms of CO_2 and oil by a molecular dynamics simulation. At the same time, the solubility calculated by simulation was compared with the related literature data, which had good agreement and verified the model's reliability. The main conclusions are as follows:

(1) The miscible behaviors between CO_2 and oil can be divided into four stages: rapid diffusion, CO_2 dissolution and oil swelling, competitive adsorption and oil film detachment, and complete miscibility or dynamic equilibrium stability.

(2) The miscible capabilities between CO_2 and different oil components follow the order of octane > dodecane > eicosane. The heavy component oil of eicosane cannot be detached by relying on the static swelling effects because of the strongest adsorption energy with the quartz.

https://doi.org/10.1021/acsomega.4c00541
ACS Omega 2024, 9, 15663−15676

(3) The CO_2 diffusion coefficient perpendicular to the quartz does not increase continuously with the temperature increase due to the adsorption of oil and quartz. There is a critical temperature range of 320−340 K that makes the CO_2 dissolution, swelling, and oil fluidity achieve the optimum.

(4) The addition of a small amount of CH_4 can promote miscibility in the CO_2−oil interface. However, it is not conducive to oil film detachment, as the interaction energy between the quartz and oil will increase with the CH_4 content.

AUTHOR INFORMATION

Corresponding Authors

Fangna Liu − *Key Laboratory of CCUS and EOR of ShaanXi Province, Research Institute of Shaanxi Yanchang Petroleum (Group) Co., Ltd., Xi'an 710065, China*; orcid.org/0009-0006-2262-975X; Email: liufangna163@163.com

Xiangzeng Wang − *Key Laboratory of CCUS and EOR of ShaanXi Province, Shaanxi Yanchang Petroleum (Group) Co., Ltd., Xi'an 710065, China*; Email: sxycpcwxz@126.com

Authors

Hong Yang − *Key Laboratory of CCUS and EOR of ShaanXi Province, Research Institute of Shaanxi Yanchang Petroleum (Group) Co., Ltd., Xi'an 710065, China*

Quansheng Liang − *Key Laboratory of CCUS and EOR of ShaanXi Province, Research Institute of Shaanxi Yanchang Petroleum (Group) Co., Ltd., Xi'an 710065, China*

Ying Liu − *Key Laboratory of CCUS and EOR of ShaanXi Province, Research Institute of Shaanxi Yanchang Petroleum (Group) Co., Ltd., Xi'an 710065, China*

Zhenjie Yao − *Key Laboratory of CCUS and EOR of ShaanXi Province, Research Institute of Shaanxi Yanchang Petroleum (Group) Co., Ltd., Xi'an 710065, China*

Complete contact information is available at: https://pubs.acs.org/10.1021/acsomega.4c00541

Notes

The authors declare no competing financial interest.

ACKNOWLEDGMENTS

This work was supported by the National Key Research and Development Program of China under grant (2022YFE0206700).

REFERENCES

(1) Zou, C.; Zhu, R.; Wu, S.; Yang, Z.; Tao, S.; Yuan, X.; Hou, L.; Yang, H.; Xu, C.; Li, D. Types, characteristics, genesis and prospects of conventional and unconventional hydrocarbon accumulations: Taking tight oil and tight gas in China as an instance. *Acta Petrol. Sin.* **2012**, *33* (2), 173−187.

(2) Camp, W. K. Pore-throat sizes in sandstones, tight sandstones, and shales: Discussion. *AAPG Bull.* **2011**, *95* (8), 1443−1447.

(3) Blunt, M. J. Flow in porous media—pore-network models and multiphase flow. *Curr. Opin. Colloid Interface Sci.* **2001**, *6* (3), 197−207.

(4) Huang, X.; Ni, J.; Li, X.; Xue, J.; Bai, M.; Zhou, T. Characteristics and influencing factors of CO_2 flooding in different microscopic pore structures in tight reservoirs. *Acta Petrol. Sin.* **2020**, *41* (7), 853−864.

(5) Syed, F. I.; Muther, T.; Van, V. P.; Dahaghi, A. K.; Negahban, S. Numerical trend analysis for factors affecting EOR performance and CO_2 storage in tight oil reservoirs. *Fuel* **2022**, *316*, 123370.

(6) Talebian, S. H.; Sagir, M.; Mumtaz, M. An integrated property−performance analysis for CO_2-philic foam-assisted CO_2-enhanced oil recovery. *Energy Fuels* **2018**, *32* (7), 7773−7785.

(7) Shi, X.; Linghui, S.; Jianfei, Z.; Li, B.; Han, X.; Lu, H.; Jiang, C. Carbon dioxide huff-puff technology and application in tight oil horizontal wells in the northern Songliao Basin. *Acta Petrol. Sin.* **2022**, *43* (7), 998−1006.

(8) Tang, X.; Li, Y.; Han, X.; Zhou, Y.; Zhan, J.; Xu, M.; Zhou, R.; Cui, K.; Chen, X.; Wang, L. Dynamic characteristics and influencing factors of CO_2 huff and puff in tight oil reservoirs. *Pet. Explor. Dev.* **2021**, *48* (4), 946−955.

(9) Sorensen, J. A.; Kurz, B. A.; Hawthorne, S. B.; Jin, L.; Smith, S. A.; Azenkeng, A. Laboratory characterization and modeling to examine CO_2 storage and enhanced oil recovery in an unconventional tight oil formation. *Energy Procedia* **2017**, *114*, 5460−5478.

(10) Abedini, A.; Torabi, F. Oil recovery performance of immiscible and miscible CO_2 huff-and-puff processes. *Energy Fuels* **2014**, *28* (2), 774−784.

(11) Kumar, N.; Sampaio, M. A.; Ojha, K.; Hoteit, H.; Mandal, A. Fundamental aspects, mechanisms and emerging possibilities of CO_2 miscible flooding in enhanced oil recovery: A review. *Fuel* **2022**, *330*, 125633.

(12) Wang, X.; Yang, H.; Wang, W.; Yao, Z.; Liang, Q.; Liu, Y. Technology and practice of CO_2 flooding and storage in low-permeability tight reservoirs. *Pet. Geol. Recovery Effic.* **2023**, *30* (2), 27−35.

(13) Guofeng, W. Carbon dioxide capture, enhanced-oil recovery and storage technology and engineering practice in Jilin Oilfield, NE China. *Pet. Explor. Dev.* **2023**, *50* (1), 245−254.

(14) Garcia Quijada, M. Optimization of a CO_2 flood design Wesson Field-west Texas. Texas A&M University, 2006.

(15) Han, W. S.; McPherson, B. J.; Lichtner, P. C.; Wang, F. P. Evaluation of trapping mechanisms in geologic CO_2 sequestration: Case study of SACROC northern platform, a 35-year CO_2 injection site. *Am. J. Sci.* **2010**, *310* (4), 282−324.

(16) Yang, Y. Research and application of CO_2 flooding technology in extra-low permeability reservoirs of Shengli Oilfield. *Pet. Geol. Recovery Effic.* **2020**, *27* (1), 11−19.

(17) White, D. J. Weyburn Geophysical Monitoring Team. Geophysical monitoring of the Weyburn CO_2 flood: Results during 10 years of injection. *Energy Procedia* **2011**, *4*, 3628−3635.

(18) Lindeberg, E.; Grimstad, A.; Bergmo, P. A.; Wessel-Berg, D.; Torsæter, M.; Holt, T. Large scale tertiary CO_2 EOR in mature water flooded Norwegian oil fields. *Energy Procedia* **2017**, *114*, 7096−7106.

(19) Pales, A. F.; Bennett, S.. Energy technology perspectives 2020; International Energy Agency, 2020.

(20) Dai, H.; Su, Y.; Liu, J.; Gu, D.; Kuang, L.; Zou, C. Thinking of China's energy development strategy under carbon neutrality goal. *Pet. Sci. Technol. Forum* **2022**, *41* (1), 1−8.

(21) Yuan, S.; Ma, D.; Li, J.; Zhou, T.; Ji, Z.; Han, H. Progress and prospects of carbon dioxide capture, EOR-utilization and storage industrialization. *Pet. Explor. Dev.* **2022**, *49* (4), 955−962.

(22) Bachu, S. CO_2 storage in geological media: Role, means, status and barriers to deployment. *Prog. Energy Combust. Sci.* **2008**, *34* (2), 254−273.

(23) Saif, T.; Lin, Q.; Butcher, A. R.; Bijeljic, B.; Blunt, M. J. Multi-scale multi-dimensional microstructure imaging of oil shale pyrolysis using X-ray micro-tomography, automated ultra-high resolution SEM, MAPS Mineralogy and FIB-SEM. *Appl. Energy* **2017**, *202*, 628−647.

(24) Bocquet, L.; Charlaix, E. Nanofluidics, from bulk to interfaces. *Chem. Soc. Rev.* **2010**, *39* (3), 1073−1095.

(25) Prakash, S.; Piruska, A.; Gatimu, E. N.; Bohn, P. W.; Sweedler, J. V.; Shannon, M. A. Nanofluidics: Systems and applications. *IEEE Sens. J.* **2008**, *8* (5), 441−450.

(26) Holt, J. K. Methods for probing water at the nanoscale. *Microfluid. Nanofluid.* **2008**, *5* (4), 425−442.

(27) Seyyedi, M.; Sohrabi, M. Pore-scale investigation of crude oil/CO_2 compositional effects on oil recovery by carbonated water injection. *Ind. Eng. Chem. Res.* **2017**, *56* (6), 1671−1681.

(28) Li, L.; Zhou, X.; Su, Y.; et al.et al. High Temperature and High Pressure Supercritical CO_2 Flooding Experiment Based on Microfluidic Experimental Platform. *Res. Explor. Lab.* **2022**, *41* (12), 81−85.
(29) Samara, H.; Al-Eryani, M.; Jaeger, P. The role of supercritical carbon dioxide in modifying the phase and interfacial properties of multiphase systems relevant to combined EOR-CCS. *Fuel* **2022**, *323*, 124271.
(30) Zhang, X.; Su, Y.; Li, L.; Da, Q.; Hao, Y.; Wang, W.; Liu, J.; Gao, X.; Zhao, A.; Wang, K. Microscopic remaining oil initiation mechanism and formation damage of CO_2 injection after waterflooding in deep reservoirs. *Energy* **2022**, *248*, 123649.
(31) Villablanca-Ahues, R.; Nagl, R.; Zeiner, T.; Jaeger, P. Interfacial tension and phase equilibria for binary systems containing (CH_4-CO_2)+(n-dodecane; n-butanol; water). *Fluid Phase Equilib.* **2023**, *570*, 113783.
(32) Cho, J.; Park, G.; Kwon, S.; Lee, K. S.; Lee, H. S.; Min, B. Compositional modeling to analyze the effect of CH_4 on coupled carbon storage and enhanced oil recovery process. *Appl. Sci.* **2020**, *10* (12), 4272.
(33) W, T. T.; Alharthy, N.; Kazemi, H.; Yin, X.; Graves, R. M.. Hydrocarbon and non-hydrocarbon gas miscibility with light oil in shale reservoirs. In *Proceedings of the SPE Improved Oil Recovery Symposium*; SPE: Tulsa, OK,USA, 2014.
(34) Guo, P.; Xhilun, L.; et al. Influences of injection gas on physical behavior of crude. *J. Southwest Pet. Inst.* **2000**, *22* (3), 57.
(35) Cao, C.; Song, Z.; Shi, Y.; Gao, Y.; Guo, J.; Chang, X. Study on CO_2 Huff-N-Puff Enhanced Recovery Technology for Jimsar Shale Oil. *Spec. Oil Gas Reservoirs* **2023**, *30* (3), 106−114.
(36) Li, C.; Yan, K.; Yang, S.; Xia, Z.; Wang, B.; Yang, F. CO_2 Swelling and Synergistic Effect of CH_4 on Rheological Improvement of Changqing Crude Oil. *J. of Petrochem. Univ.* **2017**, *30* (5), 86−92.
(37) Wang, G. Carbon dioxide capture, enhanced-oil recovery and storage technology and engineering practice in Jilin Oilfield, NE China. *Pet. Explor. Dev.* **2023**, *50* (1), 245−254.
(38) Fang, T.; Zhang, Y.; Ding, B.; Yan, Y.; Zhang, J. Static and dynamic behavior of CO2 enhanced oil recovery in nanoslits: Effects of mineral type and oil components. *Int. J. Heat Mass Transfer* **2020**, *153*, 119583.
(39) Song, Z.; Song, Y.; Guo, J.; Zhang, Z.; Hou, J. Adsorption induced critical shifts of confined fluids in shale nanopores. *Chem. Eng. J.* **2020**, *385*, 123837.
(40) Zhang, K.; Jia, N.; Li, S.; Liu, L. Thermodynamic phase behaviour and miscibility of confined fluids in nanopores. *Chem. Eng. J.* **2018**, *351*, 1115−1128.
(41) Liu, Y.; Ma, X.; Li, H. A.; Hou, J. Competitive adsorption behavior of hydrocarbon (s)/CO_2 mixtures in a double-nanopore system using molecular simulations. *Fuel* **2019**, *252*, 612−621.
(42) Luo, Y.; Liu, X. H.; Xiao, H.; Zheng, T. Microscopic production characteristics of tight oil in the nanopores of different CO_2-affected areas from molecular dynamics simulations. *Sep. Purif. Technol.* **2023**, *306*, 122607.
(43) Wang, P.; Li, X.; Tao, Z.; Wang, S.; Fan, J.; Feng, Q.; Xue, Q. The miscible behaviors and mechanism of CO_2/CH_4/C_3H_8/N_2 and crude oil in nanoslits: A molecular dynamics simulation study. *Fuel* **2021**, *304*, 121461.
(44) Moh, D. Y.; Zhang, H.; Wang, S.; Yin, X.; Qiao, R. Soaking in CO_2 huff-n-puff: A single-nanopore scale study. *Fuel* **2022**, *308*, 122026.
(45) Szczerba, M.; McCarty, D. K.; Derkowski, A.; Kowalik, M. Molecular dynamics simulations of interactions of organic molecules found in oil with smectite: Influence of brine chemistry on oil recovery. *J. Pet. Sci. Eng.* **2020**, *191*, 107148.
(46) Mohammed, S.; Gadikota, G. The influence of CO_2 on the structure of confined asphaltenes in calcite nanopores. *Fuel* **2019**, *236*, 769−777.
(47) Sun, H.; Zhao, H.; Qi, N.; Li, Y. Effects of surface composition on the microbehaviors of CH_4 and CO_2 in slit-nanopores: a simulation exploration. *ACS Omega* **2017**, *2* (11), 7600−7608.
(48) Xue, C.; Ji, D.; Cheng, D.; Wen, Y.; Luo, H.; Li, Y. Adsorption behaviors of different components of shale oil in quartz slits studied by molecular simulation. *ACS Omega* **2022**, *7* (45), 41189−41200.
(49) Zhang, J.; Zhao, Z.; Xu, Z.; Zhang, X.; Zhang, L. Surface wettability of sandstone and shale: Implication for CO_2 storage. *Int. J. Greenhouse Gas Control* **2023**, *126*, 103917.
(50) Xue, C.; Ji, D.; Wen, Y.; Luo, H.; Zhao, Y.; Li, Y. Promising combination of CO_2 enhanced oil recovery and CO_2 sequestration in calcite nanoslits: Insights from molecular dynamics simulations. *J. Mol. Liq.* **2023**, *391*, 123243.
(51) Zhang, M.; Jin, Z. Molecular simulation on CO_2 adsorption in partially water-saturated kaolinite nanopores in relation to carbon geological sequestration. *Chem. Eng. J.* **2022**, *450*, 138002.
(52) Chilukoti, H. K.; Kikugawa, G.; Ohara, T. Structure and transport properties of liquid alkanes in the vicinity of α-quartz surfaces. *Int. J. Heat Mass Transfer* **2014**, *79*, 846−857.
(53) Santos, M. S.; Franco, L. F. M.; Castier, M.; Economou, I. G. Molecular dynamics simulation of n-alkanes and CO_2 confined by calcite nanopores. *Energy Fuels* **2018**, *32* (2), 1934−1941.
(54) Le, T.; Striolo, A.; Cole, D. R. CO_2−C_4H_{10} mixtures simulated in silica slit pores: relation between structure and dynamics. *J. Phys. Chem. C* **2015**, *119* (27), 15274−15284.
(55) Liu, B.; Shi, J.; Sun, B.; Shen, Y.; Zhang, J.; Chen, X.; Wang, M. Molecular dynamics simulation on volume swelling of CO_2−alkane system. *Fuel* **2015**, *143*, 194−201.
(56) Liu, B.; Shi, J.; Wang, M.; Zhang, J.; Sun, B.; Shen, Y.; Sun, X. Reduction in interfacial tension of water−oil interface by supercritical CO_2 in enhanced oil recovery processes studied with molecular dynamics simulation. *J. Supercrit. Fluids* **2016**, *111*, 171−178.
(57) Li, C.; Pu, H.; Zhong, X.; Li, Y.; Zhao, J. X. Interfacial interactions between Bakken crude oil and injected gases at reservoir temperature: A molecular dynamics simulation study. *Fuel* **2020**, *276*, 118058.
(58) Mohammed, S.; Mansoori, G. A. Effect of CO_2 on the interfacial and transport properties of water/binary and asphaltenic oils: insights from molecular dynamics. *Energy Fuels* **2018**, *32* (4), 5409−5417.
(59) Li, X.; Wang, S.; Feng, Q.; Xue, Q. The miscible behaviors of $C_{10}H_{22}$ ($C_7H_{17}N$)/C_3H_8 system: insights from molecular dynamics simulations. *Fuel* **2020**, *279*, 118445.
(60) Le, T.; Striolo, A.; Cole, D. R. CO_2-C_4H_{10} mixtures simulated in silica slit pores: relation between structure and dynamics. *J. Phys. Chem. C* **2015**, *119* (27), 15274−15284.
(61) Dong, X.; Xu, W.; Liu, H.; Chen, Z.; Lu, N.; Wang, W. On the replacement behavior of CO_2 in nanopores of shale oil reservoirs: Insights from wettability tests and molecular dynamics simulations. *Geoenergy Sci. Eng.* **2023**, *223*, 211528.
(62) Fang, T.; Zhang, Y.; Liu, J.; Ding, B.; Yan, Y.; Zhang, J. Molecular insight into the miscible mechanism of CO_2/C_{10} in bulk phase and nanoslits. *Int. J. Heat Mass Transfer.* **2019**, *141*, 643−650.
(63) Linstrom, P. J.; Mallard, W. G. The NIST Chemistry WebBook: A chemical data resource on the internet. *J. Chem. Eng. Data* **2001**, *46* (5), 1059−1063.
(64) *Website of calculating substance properties named AP1700*. [EB/OL] [2016−04−01]. http://www.ap1700.com/index.html.
(65) de Lara, L. S.; Michelon, M. F.; Miranda, C. R. Molecular Dynamics Studies of Fluid/Oil Interfaces for Improved Oil Recovery Processes. *J. Phys. Chem. B* **2012**, *116* (50), 14667−14676.
(66) Wang, S.; Wang, J.; Liu, H.; Liu, F. Impacts of polar molecules of crude oil on spontaneous imbibition in calcite nanoslit: a molecular dynamics simulation study. *Energy Fuels* **2021**, *35* (17), 13671−13686.
(67) Shun, W. J.; Huiqing, L.; Huiqing, L.; Zemin, J.; Gaixing, H. Molecular simulation on the detachment mechanism of residual oil with the aid of surfactant. *Acta Petrol. Sin.* **2023**, *44* (3), 518−533.
(68) Mosavat, N.; Abedini, A.; Torabi, F. Phase behaviour of CO_2−brine and CO_2−oil systems for CO_2 storage and enhanced oil recovery: experimental studies. *Energy Procedia* **2014**, *63*, 5631−5645.

https://doi.org/10.1021/acsomega.4c00541
ACS Omega 2024, 9, 15663−15676

(69) Seyyedattar, M.; Ghamartale, A.; Zendehboudi, S.; Butt, S. Assessment of CO_2-Oil swelling behavior using molecular dynamics simulation: CO_2 utilization and storage implication. *J. Mol. Liq.* **2023**, *379*, 121582.
(70) Li, Y.; Zhang, J.; Li, M. Study on Supercritical CO_2 Solubility in Heavy Oil and Heavy Oil Formation Volume Factor. *Sci. Technol. Eng.* **2013**, *13* (2), 53−57.
(71) Welker, J. R. Physical Properties of Carbonated Oils. *J. Pet. Technol.* **1963**, *15* (8), 873−876.

https://doi.org/10.1021/acsomega.4c00541
ACS Omega 2024, 9, 15663−15676